water

MDPI

Article

Research on the Characteristics of Flow Velocity of a Piped Car when Starting in a Straight Pipe Section under Different Loads

Yifan Lu, Xihuan Sun *, Yongye Li, Cheng Wang and Siyuan Tao

College of Water Resources Science and Engineering, Taiyuan University of Technology, Taiyuan 030024, China; ultimate3333373@126.com (Y.L.); liyongye@tyut.edu.cn (Y.L.); taosiyuan0603@link.tyut.edu.cn (S.T.)
* Correspondence: sunxihuan@tyut.edu.cn; Tel.: +86-13934239832

Abstract: It is of great significance to explore the flow velocity characteristics of piped cars when they are started under different loads. In this paper, the flow velocity characteristics of the water flow around a piped car when it is started in the straight pipe section are studied through physical experiments. The masses of the piped cars are 1.5 kg, 1.9 kg, and 2.3 kg, respectively. The results show that, with the increase in the load of the pipeline car, the axial flow velocity in the front section increases, the absolute values of radial flow velocity and circumferential flow velocity increase, and the gradient of flow velocity increases. The positive radial flow velocity and negative circumferential flow velocity regions increase, and the distribution of positive and negative radial flow velocities and circumferential flow velocities is obvious. The gradients of axial, radial, and circumferential flow velocities in the annular section all increase, and the contour spacing becomes smaller and more densely distributed. The absolute values of the radial and circumferential flow velocities increase. The regional demarcation of axial flow velocity in the rear section is more obvious, and the average value of axial flow velocity in the high-flow-velocity area behind the vehicle increases. Additionally, the gradient of flow velocity increases. The absolute values of radial velocity and circumferential velocity increase, the gradient of velocity increases, and the velocity distribution is obviously regional. This study supplements and improves the theoretical study of a piped car when it is started and has certain reference value for the research and application of the hydraulic transport technology of the barrel-loading pipeline.

Keywords: piped car; starting; load; flow velocity characteristics

check for updates

Citation: Lu, Y.; Sun, X.; Li, Y.; Wang, C.; Tao, S. Research on the Characteristics of Flow Velocity of a Piped Car when Starting in a Straight Pipe Section under Different Loads. *Water* **2024**, *16*, 840. https://doi.org/10.3390/w16060840

Academic Editor: Giuseppe Pezzinga

Received: 16 January 2024
Revised: 11 March 2024
Accepted: 13 March 2024
Published: 14 March 2024

Copyright: © 2024 by the authors. Licensee MDPI, Basel, Switzerland. This article is an open access article distributed under the terms and conditions of the Creative Commons Attribution (CC BY) license (https://creativecommons.org/licenses/by/4.0/).

1. Introduction

At present, energy loss in the transport industry, environmental pollution, and other issues have become significant causes for social concern. The traditional transport methods on which material transport is based are unable to meet the growing demand for transport. At present, the commonly used transportation methods have problems [1–3] such as high energy consumption and high pollution. The emergence of the hydraulic transport technology of the barrel-loading pipeline [4,5] provides a new direction for the transport of materials. The hydraulic transport of the barrel-loading pipeline is a type of transport in which the conveyed material is placed in a piped car and the material is conveyed by the differential pressure force of water flow. The hydraulic transport technology of the barrel-loading pipeline plays an extremely important role in logistics industries such as agricultural product transportation, building material transportation, and food transportation, and its unique structural composition can be suitable for the loading of liquids, solids, gases, and mixed materials in various states. A piped car is equipped with legs at both ends of the car's sealed cylinder, which reduces friction with respect to the pipe wall and avoids a direct contact reaction between the material and the conveying medium. Eills [6] investigated the motion velocity of a single piped car through model tests and found that the motion velocity of the piped car increased with the increase in the diameter of the

piped car and the Reynolds number of the water flow. Kroonenberg [7] constructed a mathematical model of a piped car moving concentrically in a straight pipe, derived the equations for the motion velocity of the piped car and the flow velocity of the ring gap flow, and verified the accuracy of the equations through model tests. Ma [8] et al. studied the gap flow characteristics of different gap ratios between a piped car and a pipe when the Reynolds number was 200 and analyzed the flow velocity of gap flow, the evolution of boundary layer flow, and the change rule of wake flow when the gap ratio changed from 0.03 to 0.3. Ihab [9] et al. used three different turbulence models to investigate the flow field characteristics of the concentric ring gap formed by a long straight cylindrical piped car and a pipeline and compared the computational accuracy of the three models. Ivanov [10] et al. explored the efficiency as well as reliability of the transmission system of a barrel-loading pipeline and proposed a series of maintenance methods for the piped car transmission system according to the actual conditions in different regions. Sultan [11] and Peng [12] et al. used numerical simulation to study the flow velocity distribution in the flow field of the ring gap of a piped car and determined the influence of the ring gap width of the piped car on the energy consumption characteristics present when moving the piped car. Cheng [13] and Jiang [14] et al. studied the influence of the front and rear sections of a piped car on the distribution of the flow field around the piped car and obtained the distribution law of the influence of the water flow line around the piped car in the event of a sudden change of the sections in the front and rear of the piped car. Paul [15] et al. studied the influence of factors such as piped car spacing, diameter ratio, and length-to-diameter ratio on the energy consumption of a piped car during transport and obtained the optimal model of a piped car through optimal cost analysis. Taimoor [16,17] et al. used numerical simulation to investigate the hydraulic characteristics of individual piped cars during the movement of straight, curved, and vertical pipe sections and optimized the transmission system based on the principle of minimum cost. Lenau [18] et al. investigated the critical start-up flow velocity that causes a cylindrical piped car to remain inclined under the action of an obstacle. Due to instrumentation limitations, the hydraulic characteristics of the pipe flow field were not fully ascertained from the model tests. Zhang [19] et al. used the method of fluid–solid coupling to study the motion characteristics of piped cars with different diameter-to-length ratios and the hydraulic characteristics of the water flow in the pipeline and found that the dynamic boundary ring gap flow around the piped car was influenced by both the upstream and downstream flow fields in the pipeline and the structure of the pipeline itself. Zhao [20,21] et al. established a transient model for the movement of a piped car in a pipeline and investigated the vortex structure and pulsation structure of the flow field around the piped car through numerical simulation. Turkowski [22] et al. used the theoretical method of obtaining an optimal solution to establish a model of a piped car in a pipeline, emphasized the cost-effectiveness of a piped car in actual operation, and finally proposed an optimal model of a piped car. Asim [23] et al. investigated the influence of the shape of a piped car on the flow field characteristics of a pipeline and determined the optimal shape of the piped car by comparing the flow field velocity and pressure distribution of the three different shapes of the designed piped car. Yang [24] et al. used a combination of numerical simulation and physical experiments to analyze the distribution of the flow velocity and pressure around a piped car and to obtain the distribution law of shear stress on the wall of the piped car. Abushaala [25] et al. studied a piped car in horizontal, vertical, and curved pipelines through numerical simulation to obtain the distribution law of water flow velocity and pressure around the piped car in various pipelines. Ulusarslan [26–28] et al. investigated the effects of the mass and diameter ratio of a piped car and the flow rate in a pipe on the energy loss of the piped car during transportation and determined the effects of different pipe flow rates, piped car masses, and diameter ratios of the piped car on the energy loss of the piped car during transportation.

With the in-depth study of the hydraulic transport technology of a barrel-loading pipeline, the study of hydraulic characteristics of piped car starting has gradually become a focus of research. When a piped car starts, the flow field distribution is more complex.

Load is an important factor affecting the starting of a piped car. The change in load will affect the flow rate of the starting of the piped car, and the change in flow rate will affect the flow velocity distribution of the flow field. At present, there are few studies on the influence of load on piped cars when they start. Therefore, this paper uses the method of physical testing to study and analyze the flow velocity characteristics of a piped car under different loads when starting in straight pipe sections and determines the flow velocity distribution of a piped car when starting under different load conditions so as to provide theoretical support for the study of the energy consumption of piped cars at start-up and provide a certain theoretical reference for the industrial application of this technology.

2. Experimental Design

2.1. Structure of the Piped Car

A piped car is mainly composed of a barrel, a sealing cap, and legs. The barrel is made of plexiglass; it has a wall thickness of 5 mm and is hollow so that it can hold material. The length of the barrel selected for this test was 150 mm, and the diameter was 75 mm Diameter. The sealing cap was made of a thin glass plate with a thickness of 10 mm and was connected to the barrel to form an airtight cylindrical barrel. In order to keep the piped car concentric with respect to the pipe when it is started inside the pipe, three legs were installed at each end of the piped car, with an equal spacing of 120° between the legs. The legs are cylindrical, with a diameter of 7 mm. The structure of the piped car is shown in Figure 1.

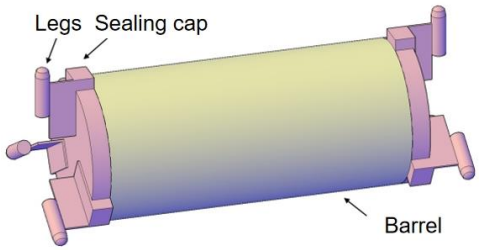


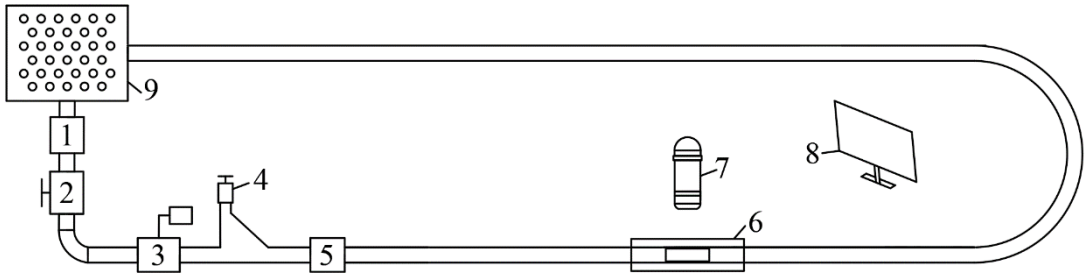
Figure 1. Schematic diagram of the structure of the piped car.

2.2. Test System

The test system consists of a power and regulation system, a putting and receiving system, a test piping system, and a measurement system. The power system is a centrifugal pump, the regulating system consists of a gate valve and an electromagnetic flowmeter, and the test piping system consists of a plexiglass round tube with an inner diameter of 100 mm and a thickness of 5 mm connected by a flange. The measurement system consists of a laser velocimetry device, a computer, and a rectangular water tank, among which the laser velocimetry device includes a particle image velocimeter (PIV), a laser, a camera, and a coordinate frame. Table 1 lists the PIV parameters. Before the test, the rectangular water tank was filled with water to prevent laser reflection, and the tracer particles were added to the water tank with a steady flow plate. The laser and camera were mounted on the coordinate frame, which was precisely moved by a computer to control the opening and closing times of the laser, and a particle image velocimeter (PIV) was used to capture the motion images of the tracer particles inside the pipe. Finally, the particle images were converted into the three-dimensional flow velocity in the right-angle coordinate system by the computer's post-processing software PIVlab 2.63.0.0. Figure 2 shows the layout of the test system and a diagram of the PIV system used.

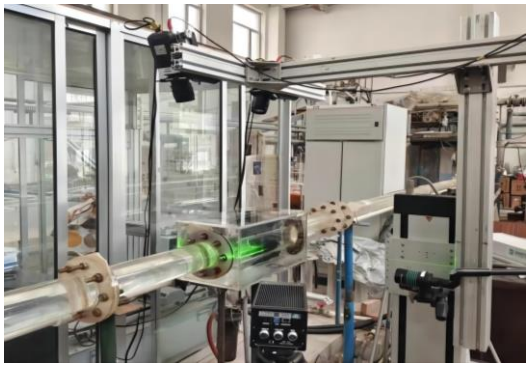
Table 1. Experimental settings for PIV measurements.

Experimental Setting	Main Parameter
Illumination	Dual Power Nd-YLF Laser (2 × 30 mJ)
Camera lens	2 Imager pro HS cameras
Image dimension	2016 × 2016 pixels
Interrogation area	32 × 32 pixels
Time between pulses	5 × 103 μs
Seeding material	Polystyrene particles diameter 55 μm
Resolution ratio	39.68 μm/pixel



①: Centrifugal pump; ②: gate valve; ③: electromagnetic flow meter; ④: piped car drop-off port; ⑤: water pipeline; ⑥: rectangular water tank; ⑦: laser velocimetry device; ⑧: computer; ⑨: water tank.

(**a**)



(**b**)

Figure 2. Layout of test system and schematic diagram of the PIV system used: (**a**) Layout of test system; (**b**) schematic diagram of the PIV system used.

2.3. Test Section and Point Placement

Taking the direction of water flow as the positive direction, the test pipe section was divided into three regions: the front of the car, the ring gap, and the rear of the car. In the front-of-the-car area, test sections #1, #2, and #3 were arranged; the distances from the pipeline car were 50 mm, 30 mm, and 10 mm, respectively. Three test sections, #4, #5, and #6, were arranged in the ring gap area; section #5 was located in the middle of the body of the piped car, and section #4 and section #6 were 2/5 of the car's length away from section #5. Three test sections, #7, #8, and #9, were arranged in the rear area of the car; the distances from the pipeline car were 40 mm, 70 mm, and 110 mm, respectively, and the arrangement of the test sections is shown in Figure 3a. Each test point adopts the arrangement method of using polar coordinates, with each polar axis spaced at 30°, and 12 polar axes were arranged. With the pipeline axis at the center of the circle, the arrangement of five different

radii of the measuring ring, and the intersection of the measuring ring and the polar axis for the test point, each test section layout consisted of 60 measurement points. At the piped car ring gap, the formula for calculating the radius of the measuring ring is $D/2 + d/5$, $D/2 + 2d/5$, $D/2 + d/2$, $D/2 + 3d/5$, $D/2 + 4$d$/5$, where the outer diameter of the piped car is D, and the inner diameter of the pipeline is Dg, and the gap width is $d = (Dg - D)/2$. The arrangement of the measurement points for the test section is shown in Figure 3b,c.

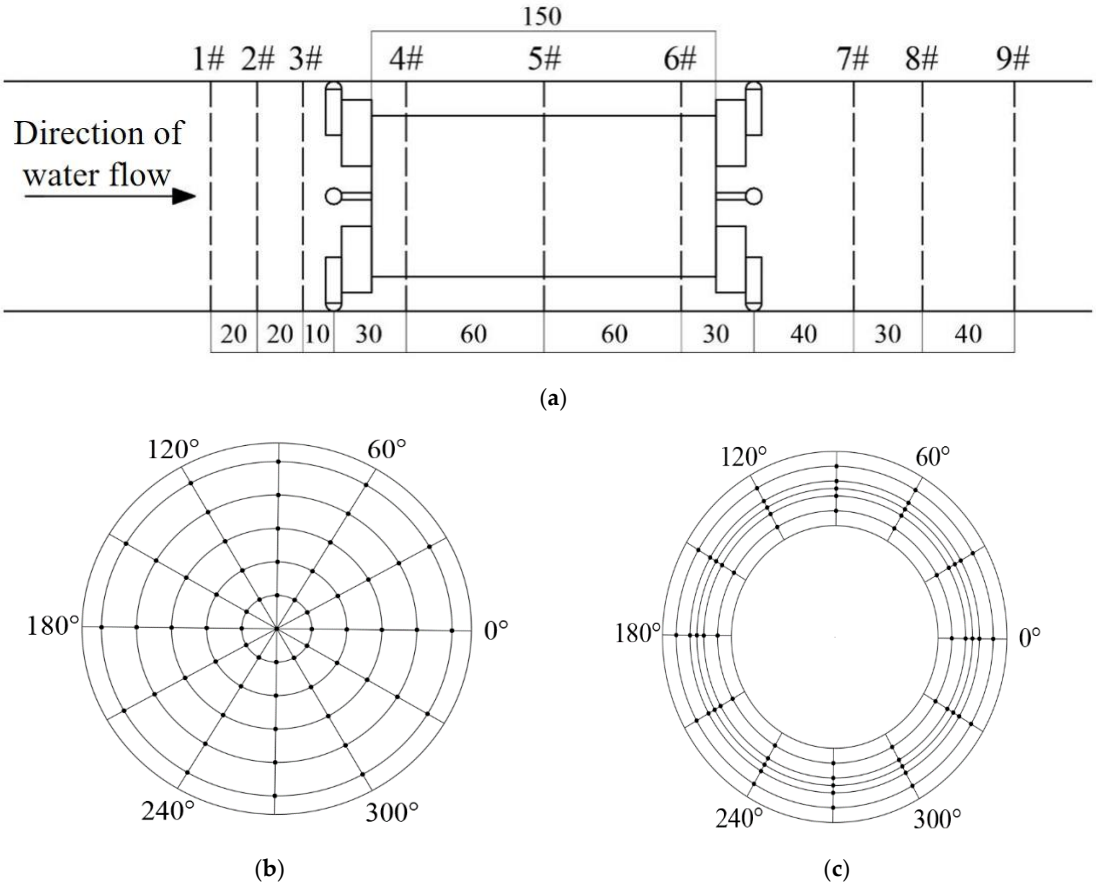


Figure 3. Schematic diagram of measurement point layout: (**a**) the arrangement of the test sections (unit: mm), (**b**) the layout of measurement points in the front and rear sections of the piped car, and (**c**) the layout of measurement points in the ring gap section.

2.4. Test Conditions

Since this test took the conveying load of the piped car to be the main influencing factor, scenarios involving a piped car with loads of 1.5 kg, 1.9 kg, and 2.3 kg and $L \times D$ = 150 mm × 75 mm were selected as the test models for this test. The three load values correspond to three situations: the piped car is not loaded with materials, the materials are half-loaded, and the materials are fully loaded.

3. Analysis of the Test Results

3.1. Characteristics of Flow Velocity in the Front Section of the Piped Car When Starting under Different Loads

The axial, radial, and circumferential flow velocity distributions in the section in front of the car (sections #1, #2, and #3) when the piped car starting in the straight pipe section under different loads are shown in Figures 4–6. The figures provide the following findings:

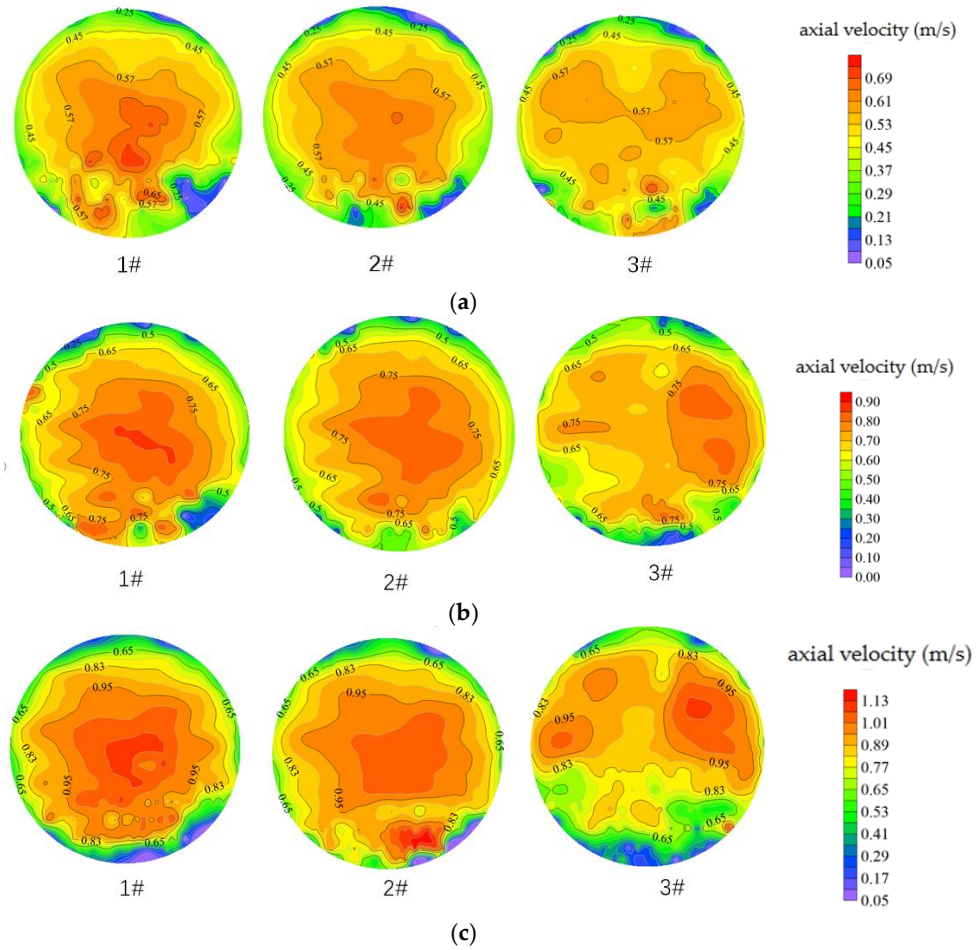


Figure 4. Axial velocity distribution in the front section of the piped car when starting under different loads: (**a**) M = 1.5 kg; (**b**) M = 1.9 kg; (**c**) M = 2.3 kg.

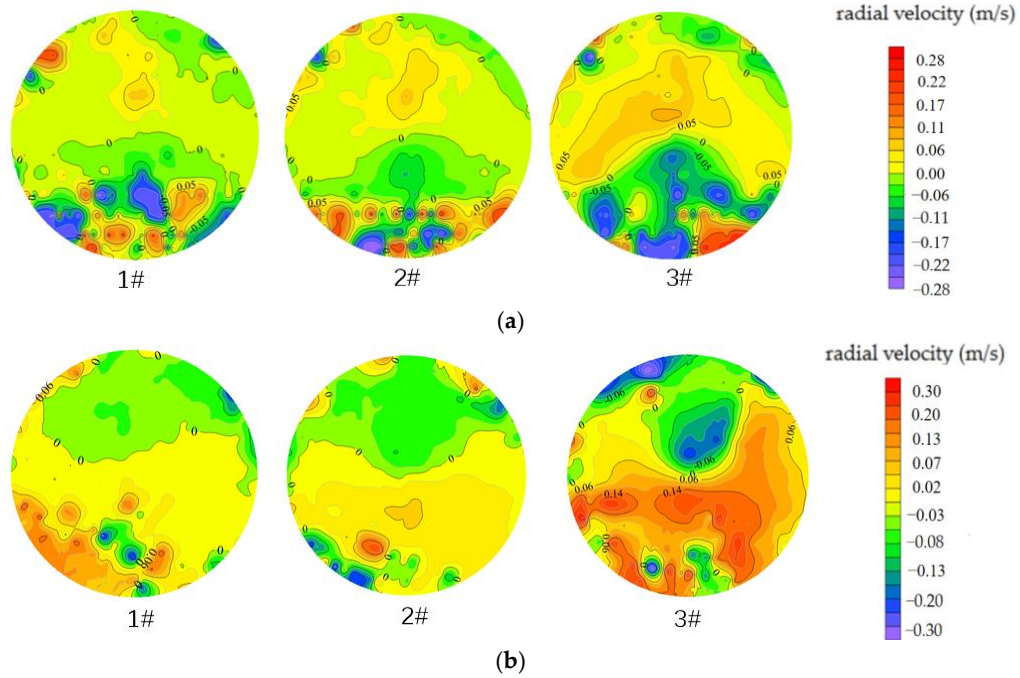
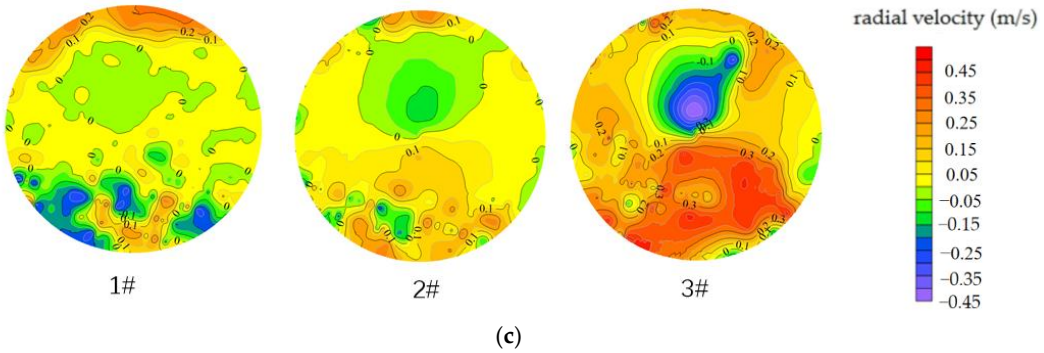


Figure 5. *Cont.*



(**c**)

Figure 5. Radial velocity distribution in the front section of the piped car when starting under different loads: (**a**) M = 1.5 kg; (**b**) M = 1.9 kg; (**c**) M = 2.3 kg.

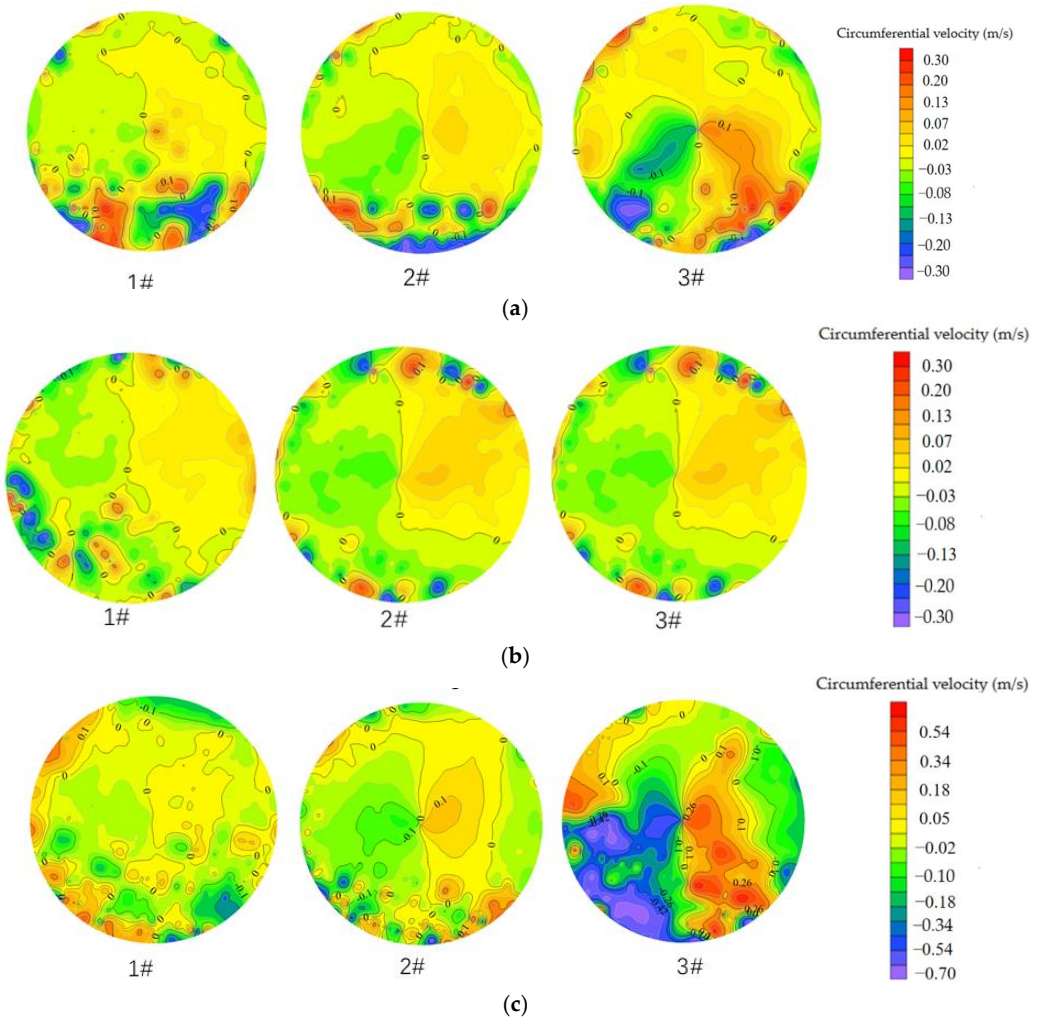


Figure 6. Circumferential velocity distribution in the front section of the piped car when startingunder different loads: (**a**) M = 1.5 kg; (**b**) M = 1.9 kg; (**c**) M = 2.3 kg.

(1) The axial velocity distribution in the front section of the piped car is between 0.00 m/s and 1.13 m/s, and all the values are positive, indicating that the axial velocity in front of the car is the same as that in the water flow direction when the piped car starts. At the positions of section #1 and section #2 in front of the car, the axial velocity had an approximately concentric-ring-shaped distribution, the axial velocity was the largest at the center of the pipe axis, the axial velocity gradually decreased from the center of the pipe axis along the pipeline radius direction, and the axial velocity was the

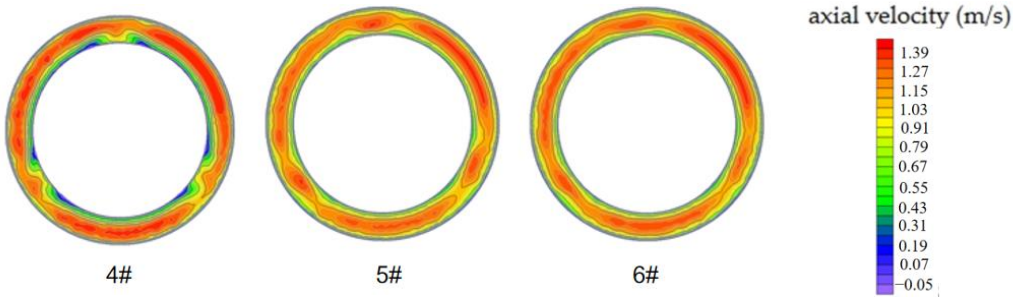
smallest at the wall of the pipe. This result is due to the fact that near the wall of the pipe, the flow velocity of the water is reduced due to viscous forces. When the piped car starts, the water flows into the downstream section of the pipe from the front of the car, and the water does not flow back, so the axial flow rate is less affected by the pipeline car in the positions of section #1 and section #2 in front of the car. In the position of section #3 in front of the car, the axial velocity has a rotationally symmetric distribution and is higher in the region with a measuring ring radius of 18 mm–36 mm and a polar axis of 0°–60°, while it is lower in the region with a measuring ring radius of 27 mm–36 mm and polar axes of 85°–95°, 205°–215°, and 325°–335°. Since section #3 is located 10 mm from the front foot of the piped car, the water flow is blocked by the foot of the piped car and the barrel, converting part of the kinetic energy into pressure energy, causing the axial velocity to decrease, and changing the distribution law of the flow velocity, so at the position of section #3, the piped car has a greater impact on axial velocity when it is started. For the piped car with model characteristics of $L \times D$ = 150 mm × 75 mm, the axial velocity in section #1, section #2, and section #3 in front of the car increases when the load is increased, and the gradient of the flow velocity change increases. When the load of the piped car increases from 1.5 kg to 2.3 kg, the maximum value of axial flow velocity increases by 57.53%, and the maximum value of flow velocity gradient increases by 77.1%, indicating that the increase in load has a greater effect on the axial velocity in the section in front of the car when the piped car is started.

(2) The radial velocity distribution in the front section of the piped car is between −0.45 m/s and 0.50 m/s, and the flow velocity is both positive and negative. The positive radial velocity ranges from the center of the section along the radius to the wall of the pipeline, and the negative radial velocity ranges from the wall of the pipeline to the center of the section. At the position of section #1 and section #2 in front of the car, the positive radial velocity at the center of the sections is larger, and the negative radial velocity is smaller. Along the radius of the section from the center of the circle to the pipe wall, the absolute value of the radial velocity gradually decreases due to the influence of the viscous force on the pipe wall. At the position of section #3 in front of the car, the absolute value of radial velocity increases significantly, and the maximum radial velocity increases by 76.47% compared with the maximum radial velocity of section #2. The positive flow velocity area of the radial velocity of section #3 increases, which accounts for about 77.93% of the total area of section #3. For the piped car with $L \times D$ = 150 mm × 75 mm, when the values of load are 1.9 kg and 2.3 kg, the positive radial velocity of section #1, section #2, and section #3 in front of the car is centrally distributed in the lower side area of the sections, the negative radial velocity is centrally distributed in the upper side area of the sections, and water flows from the upper side of the pipeline to the lower side of the pipeline; when the load is 1.5 kg, the distribution of positive and negative areas of radial flow velocity is opposite: the radial flow velocity in the upper side area of section #1, section #2, and section #3 in front of the car is positive; the radial flow velocity in the lower side area is negative; and water flows from the lower side of the pipeline to the upper side of the pipeline. When the piped car models are the same and the load is increased, the absolute value of radial velocity in section #1, section #2, and section #3 increases, and the positive radial velocity area increases. At the position of section #1 and section #2, with the increase in the load of the piped car, the boundary of the distribution of the positive and negative radial flow velocity area gradually becomes fuzzy. At the position of section #3, when the load was increased from 1.5 kg to 1.9 kg, the absolute value of radial flow velocity increased by 0.02 m/s, and the change in flow velocity was small; when the load was increased from 1.9 kg to 2.3 kg, the absolute value of radial velocity increased by 0.15 m/s, and the change in flow velocity was significant. These results show that the increase in load has a greater effect on the radial velocity in the section in front of the car when the piped car starts.

(3) The circumferential velocity distribution in the front section of the piped car is between −0.70 m/s and 0.62 m/s, and the variation in circumferential velocity is larger than that for radial velocity. The absolute value of the circumferential velocity is the largest at the center of the pipe axis, and the absolute value of the velocity gradually decreases when moving from the center of the pipe axis to the pipe wall along the radius direction. At the position of section #1 and section #2, the sections are divided into two areas with the 90° polar axis and 270° polar axis as the dividing line, defining the area from 90° to 270° along the anticlockwise direction of the polar axis as the left area and the area from 270° to 90° along the anticlockwise direction of the polar axis as the right area. The negative circumferential velocity of section #1 and section #2 is mainly distributed in the left area, and the flow is in the anticlockwise direction; the positive circumferential velocity is mainly distributed in the right area, and the flow is in the clockwise direction. At the position of section #3 in front of the car, the absolute value of the circumferential velocity increases significantly, and the variation gradient of velocity is larger. When the piped car types are the same and the load increases, the absolute value of the circumferential velocity increases, and the variation gradient of velocity Increases in section #1, section #2, and section #3. At the position of section #1 in front of the car, when the values of load are 1.5 kg and 1.9 kg, the circumferential velocity is distributed between −0.30 m/s and 0.30 m/s, the positive circumferential velocity is mainly distributed in the right area, and the negative circumferential velocity is mainly distributed in the left area; when the load is 2.3 kg, the circumferential velocity is distributed between −0.70 m/s and 0.70 m/s, the trend of increasing flow velocity is significant, and the region of negative circumferential velocity increases. At the position of section #2 and section #3 in front of the car, the distribution law of circumferential velocity is similar, the absolute value of circumferential velocity increases, and the variation gradient of velocity increases. The positive circumferential velocity area of section #2 increases by 46%, and the flow tends to increase in the clockwise direction. The negative circumferential flow velocity area of section #3 increases by 34%, and the flow tends to increase in the counterclockwise direction. These results show that the increase in load has a greater effect on the circumferential velocity in front of the piped car when the piped car starts.

3.2. Characteristics of Flow Velocity in the Ring Gap Section when Starting the Piped Cars with Different Loads

The axial, radial, and circumferential flow velocity distributions in the ring gap sections (sections #4, #5, and #6) when starting the piped cars with different loads are shown in Figures 7–9. The figures reveal the following:



(**a**)

Figure 7. *Cont.*

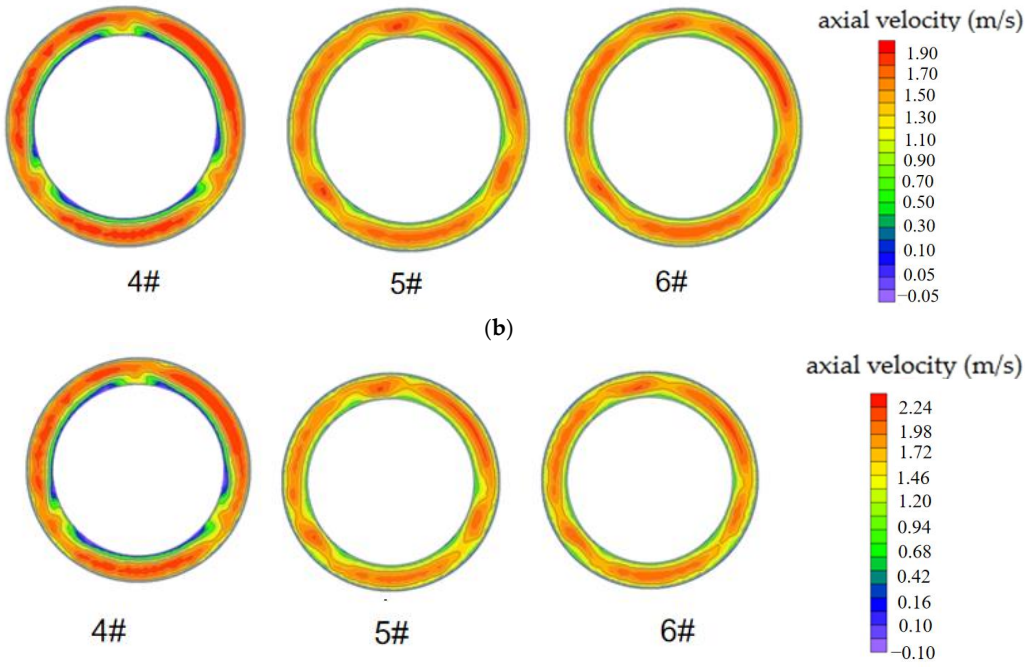


Figure 7. Axial velocity distribution in the ring gap section when starting the piped car under different loads: (**a**) M = 1.5 kg; (**b**) M = 1.9 kg; (**c**) M = 2.3 kg.

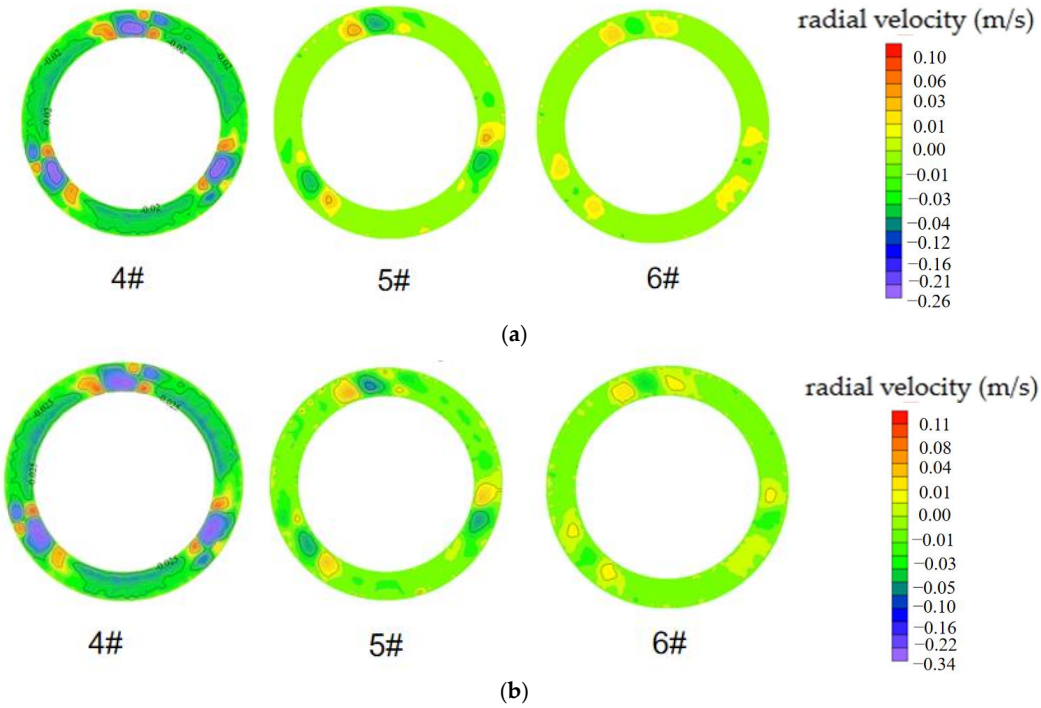
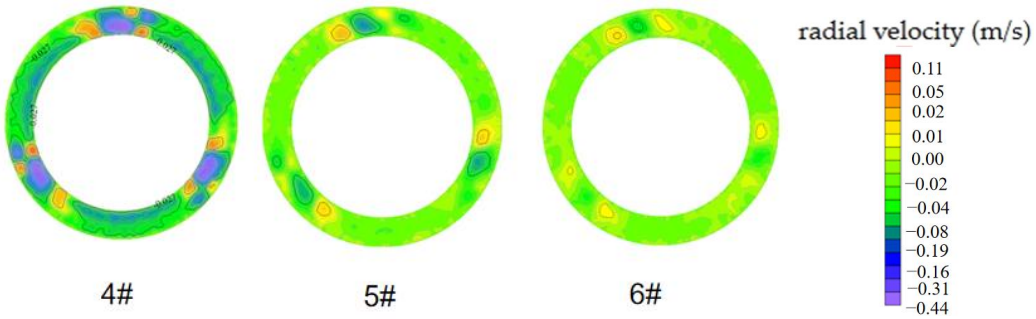
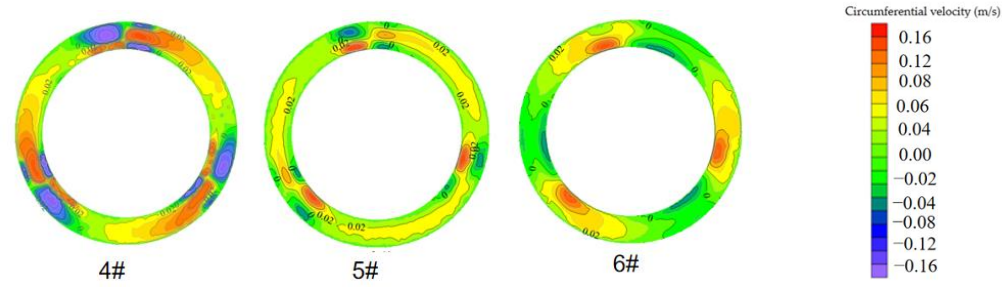


Figure 8. *Cont.*

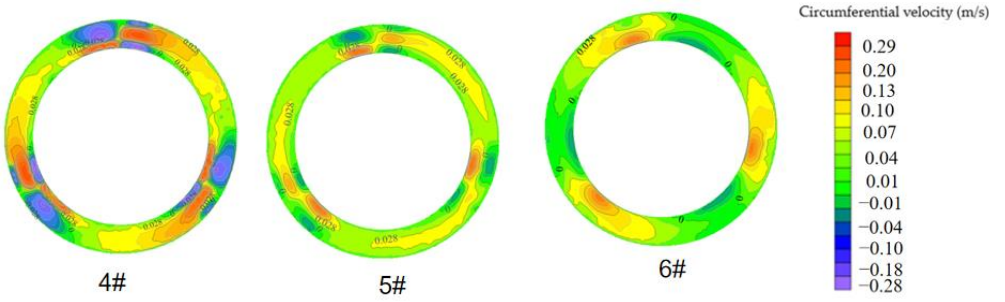


(**c**)

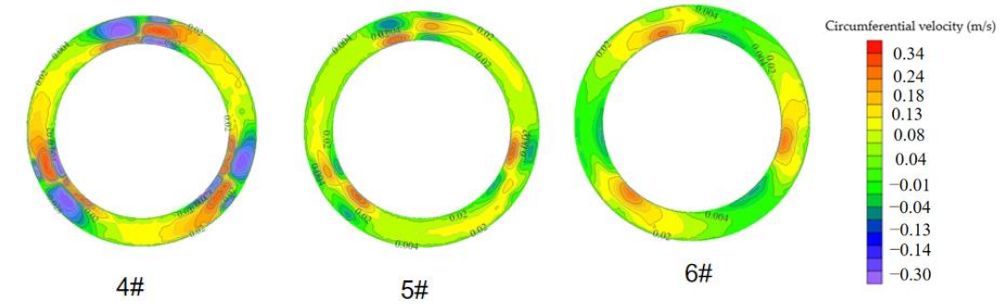
Figure 8. Radial velocity distribution in the ring gap section when starting the piped car under different loads: (**a**) M = 1.5 kg; (**b**) M = 1.9 kg; (**c**) M = 2.3 kg.



(**a**)



(**b**)



(**c**)

Figure 9. Circumferential velocity distribution in the ring gap section when starting the piped car under different loads: (**a**) M = 1.5 kg; (**b**) M = 1.9 kg; (**c**) M = 2.3 kg.

(1) The axial velocity in the ring gap section is distributed between −0.20 m/s and 2.37 m/s, the positive axial velocity is the same as that in the water flow direction, and the negative axial velocity is opposite to the water flow direction. The axial velocity is symmetrically distributed around the center of the section at 120°, and the flow velocity distribution is regionally obvious, with the maximum axial velocity in the center of the ring gap, which gradually decreases along the radius to the outer wall of the piped car and the inner wall of the pipeline. When the water flows from the

front of the car area into the ring gap area, the direction of water flow changes due to the blocking effect of the piped car barrel, the water cross section decreases, and the axial velocity in the ring gap increases and is significantly larger than the axial velocity of the front section of the car. At the position of section #4 of the ring gap, the water flow just enters the ring gap area, the development is not sufficient over a short period of time, and the variation gradient of axial velocity is larger. The axial velocity is distributed between 1.39 m/s and 2.37 m/s; the axial velocity near the wall of the piped car body is smaller and has a negative value, and the flow velocity is distributed between −0.20 m/s and 0.68 m/s. The water flow is blocked by the barrel of the piped car, the cross section of the water suddenly shrinks, and the axial velocity in the center of the ring gap increases; the water flow near the wall of the piped car body is closer to the front legs of the pipeline car, and the formation of disturbed flow velocity under the influence of the legs is small. At the position of section #5 of the ring gap, the water flow develops more fully, the positive axial velocity decreases, the negative axial flow velocity disappears, and the variation gradient of velocity decreases. At the position of section #6 of the ring gap, the axial velocity decreases, and the regional distribution of flow velocity becomes more obvious. For the piped car for which $L \times D$ = 150 mm × 75 mm, when the load is increased from 1.5 kg to 2.3 kg, the average axial flow velocity of sections #4, #5, and #6 increases by about 55%, and the average flow velocity gradient increases by about 63%. Furthermore, the maximum value of axial velocity increases, the minimum value changes less, the variation gradient of velocity increases, and the contour spacing becomes smaller and has a more intense distribution. These results show that the increase in load has a greater effect on the axial velocity in the ring gap section when the piped car starts.

(2) The radial velocity in the ring gap section is distributed between −0.55 m/s and 0.19 m/s, the positive radial velocity ranges from the center of the section along the radius to the position of the pipeline wall, and the negative radial velocity ranges from the position of the pipeline wall to the position of the center of the section. Negative radial velocity accounted for a larger area of the ring gap section, indicating that most of the water flowed from the piped car body wall to the inner wall of the pipeline. At the position of section #4 of the ring gap, the difference between the maximum and minimum values of radial velocity is large, and the variation gradient of velocity is large. At the position of section #5 in the ring gap, the magnitude of the change in radial velocity decreases, and the distribution of flow contours is more sparse, indicating that the flow is more fully developed by the time it reaches section #5. At the position of section #6 in the ring gap, the variation gradient of radial velocity decreases, and the flow velocity is mainly negative, indicating that the radial velocity is directed toward the center of the circle along the radius direction. At this time, the water flow is about to flow out of the ring gap region, a process that is strongly influenced by the piped car barrel. The piped car's rear-facing legs will also have a disruptive effect at the same time, causing the section of the ring gap flow radial velocity to be directed toward the center of the circle. For the piped car model for which $L \times D$ = 150 mm × 75 mm, the negative radial velocity decreases with the increase in load at the position of section #4, and the trend of decreasing gradually increases. At the positions of section #5 and section #6, the radial velocity increases as the piped car load increases, and the variation gradient of velocity increases. This shows that the increase in load has a greater effect on the radial velocity in the ring gap section when the piped car starts.

(3) The circumferential velocity in the ring gap section is distributed between −0.30 m/s and 0.34 m/s. The circumferential velocity in the ring gap area is mainly positive, and most of the water flows in the clockwise direction along the circumferential tangent. The circumferential velocity at sections #4, #5, and #6 of the ring gap is symmetrically distributed, with a rotation of 120° around the centers of the sections. At the position of section #4 in the ring gap, the variation gradient of circumferential

velocity is larger, and the water flow, when entering the ring gap area of the piped car, collides with the connection between the front support piece and the legs of the piped car, greatly impacting the circumferential rate. As section #4 is the section at the position where the water flow just enters the ring gap area, the water flow is not yet fully developed, and the change in circumferential velocity is drastic. At the position of section #5 in the ring gap, the distribution law of circumferential velocity is similar to that of section #4, the negative circumferential velocity area decreases, the variation gradient of velocity decreases, and the influence of the piped car's front legs and material barrel on the circumferential velocity decreases. At section #6, where the water is about to flow out of the ring gap area, the circumferential velocity is mainly affected by the rear legs of the piped car, causing the positive and negative circumferential velocity distribution areas to change significantly. For the pipeline car model for which $L \times D$ = 150 mm × 75 mm, with the increase in load, the piped car has a greater impact on the circumferential velocity in the ring gap section when starting.

3.3. Characteristics of Flow Velocity in the Rear Section of the Piped Car When Starting under Different Loads

The axial, radial, and circumferential flow velocity distributions in the section behind the car (sections #7, #8, and #9) when the piped car starts in the straight pipe section under different loads are shown in Figures 10–12. The figures reveal the following:

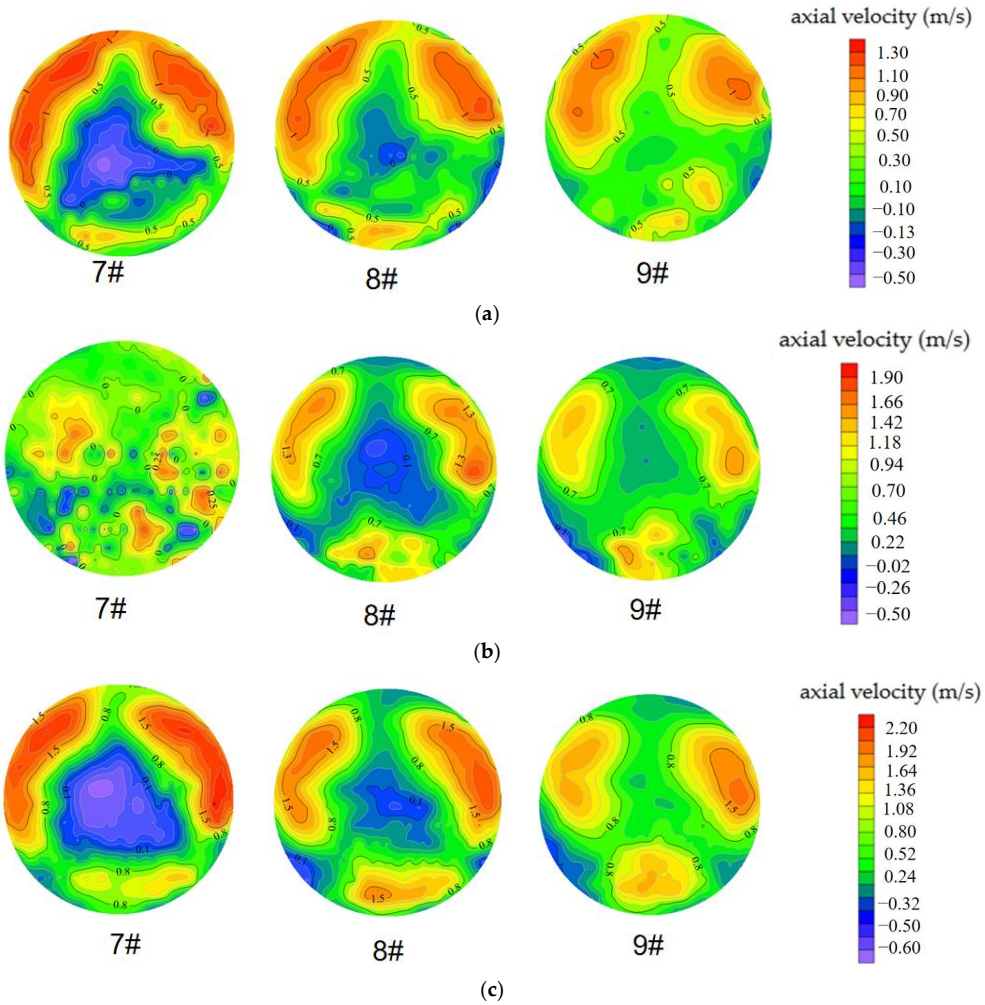


Figure 10. Axial velocity distribution in the rear of the piped car when starting under different loads: (**a**) M = 1.5 kg; (**b**) M = 1.9 kg; (**c**) M = 2.3 kg.

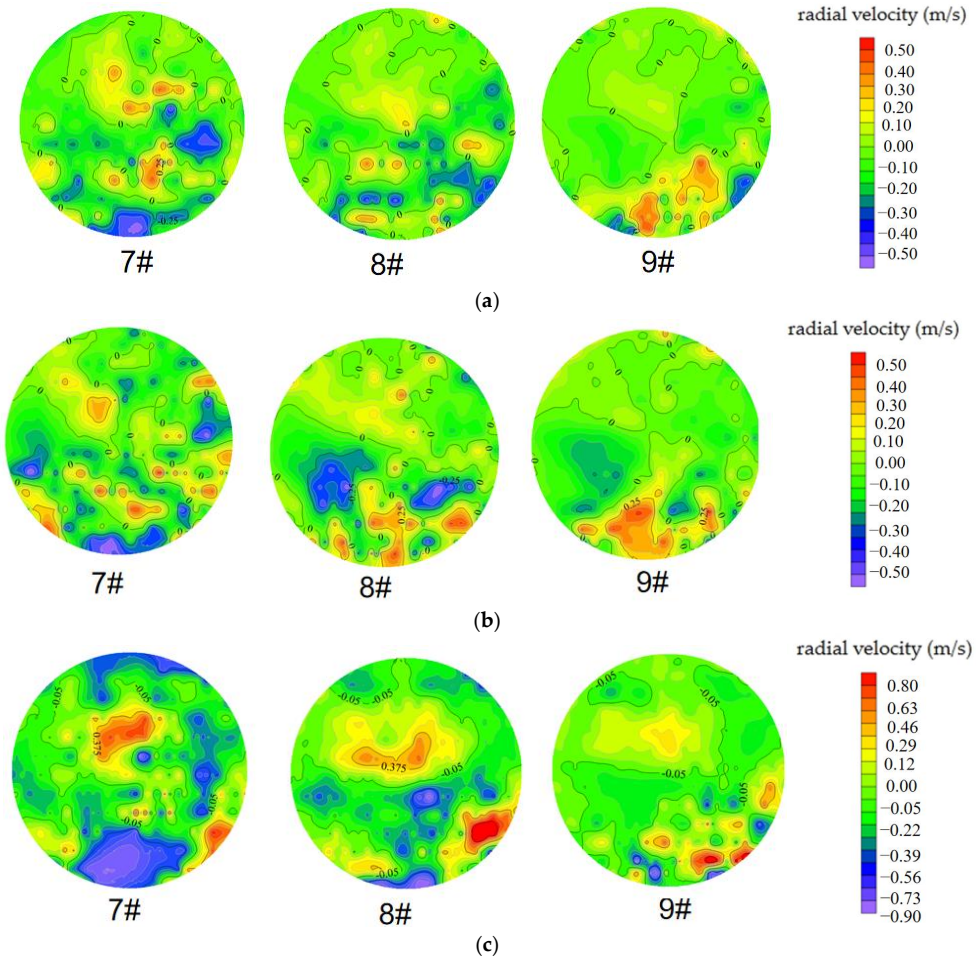


Figure 11. Radial velocity distribution in the rear of the piped car when starting under different loads: (**a**) M = 1.5 kg; (**b**) M = 1.9 kg; (**c**) M = 2.3 kg.

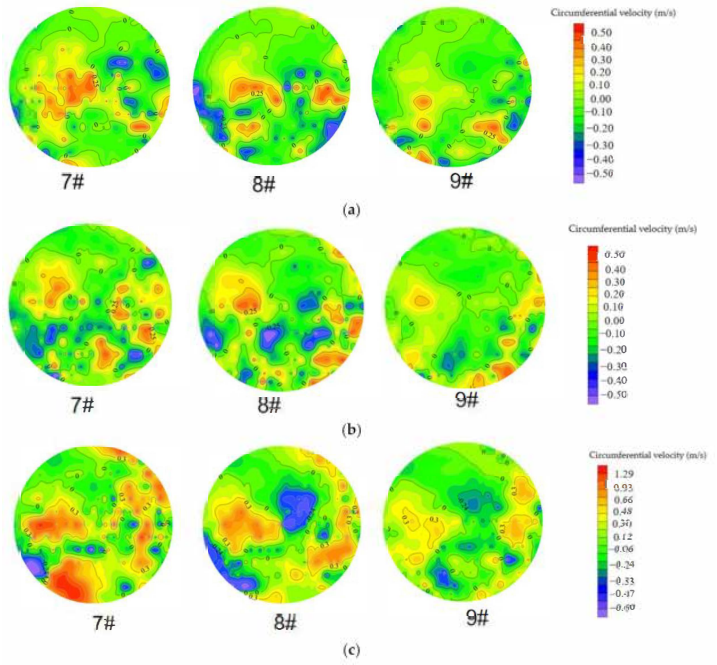


Figure 12. Circumferential velocity distribution in the rear of the piped car when starting under different loads: (**a**) M = 1.5 kg; (**b**) M = 1.9 kg; (**c**) M = 2.3 kg.

(1) The axial velocity in the rear section of the piped car is distributed between −0.60 m/s and 2.20 m/s, the positive axial velocity is the same as the water flow direction, and the negative axial velocity is the opposite of the water flow direction. The axial velocities in section #7, section #8, and section #9 are basically rotationally symmetric around the sections' centers at 120°. When the water flows into the area at the rear of the car, the water cross section increases, and the average axial velocity of section #7, section #8, and section #9 behind the car is larger than the starting flow velocity of the piped car, and the axial flow velocity in the low-flow zone of section #7 at the rear of the car is distributed between −0.60 m/s and 0.00 m/s, which accounts for about 19% of the total area of section #7. When the water flows into the area at the rear of the car, the average axial velocity in section #7, section #8, and section #9 behind the car is larger than that of the water flow when the piped car starts because of the increase in the water cross section, and the axial velocity in the low-flow zone at section #7 is distributed between −0.60 m/s and 0.00 m/s, which accounts for about 19% of the total area of section #7. This indicates that as the water flow enters the rear area of the car, the water cross section increases, and a portion of the water flowing in will flow back behind the piped car, resulting in a negative axial velocity. At the position of section #8 at the rear of the car, the average axial velocity decreases in the high-flow-velocity zone, while the average axial velocity increases in the low-flow-velocity zone, and the variation gradient of velocity decreases. At the position of section #9 at the rear of the car, the average axial velocity in the high-flow-velocity zone at the rear of the car decreases, the negative axial velocity disappears, the variation gradient of velocity decreases, and the demarcation between the zones is gradually blurred. For the piped car for which $L \times D$ = 150 mm×75 mm, the load increased from 1.5 kg to 2.3 kg, the average axial flow velocity in the high-flow-velocity area behind the vehicle increased by 47.63%, and the average flow velocity gradient increased by 55.5%. Additionally, the average value of axial velocity in the low-flow velocity zone at the rear of the car changed less, and the variation gradient of velocity change increased. This shows that the increase in load has a greater effect on the axial velocity at the rear of the car when the piped car starts.

(2) The radial velocity in the rear section of the piped car is distributed between −0.45 m/s and 0.50 m/s, the positive radial velocity ranges from the center of the section along the radius to the pipe wall position, and the negative radial velocity spans from the pipe wall position to the center of the section. At the position of section #7 at the rear of the piped car, the water flow just enters the area behind the car; at this time, the water flow is affected by the piped car's rear-facing legs and the piped car ring gap area, the absolute value of radial flow rate is large, the flow rate changes drastically, and there is no obvious regional distribution of positive and negative radial velocity. At the positions of section #8 and section #9 at the rear of the car, the absolute value of radial velocity decreases, and the variation gradient of velocity decreases. For the piped car for which $L \times D$ = 100 mm × 75 mm, the regional distribution of positive and negative radial velocity is obvious with the increase in the load of the pipeline car. This indicates that the increase in load has a greater effect on the radial velocity at the rear of the car when the piped car starts.

(3) The circumferential velocity in the rear section of the piped car is distributed between −0.60 m/s and 1.29 m/s. When the value of the circumferential velocity is positive, the water flows clockwise along the circumferential tangent line; when the value of the circumferential velocity is negative, the water flows anti-clockwise along the circumferential tangent line. Due to the sudden expansion of the water cross section, the water flow is blocked by the legs of the piped car, resulting in large disturbances, and the change in circumferential velocity becomes more intense. At the position of section #7 at the rear of the piped car, the variation gradient of the circumferential velocity is larger. The absolute value of the circumferential velocity at section #8 decreases, and the variation gradient of the circumferential velocity decreases; the

change rule of the circumferential velocity at section #9 is similar to that at section #8. This shows that as the distance from the piped car increases, the influence of the piped cars' legs on circumferential velocity gradually decreases. For the piped car for which $L \times D$ = 150 mm × 75 mm, as the piped car load increases, the area of the positive circumferential velocity region increases, and the regional distribution of the flow velocity is more obvious. This shows that the increase in load has a greater effect on the circumferential velocity at the rear of the car when the piped car starts.

4. Conclusions

1. Characteristics of flow velocity in front of the car: The axial velocity of the front section is distributed between 0.00 m/s and 1.13 m/s, and all of these values are positive. When the load of the piped car increases, the axial velocity increases, and the variation gradient of velocity increases. The radial flow velocity of the front section is distributed between −0.45 m/s and 0.50 m/s, and the flow velocity is both positive and negative. When the load of the piped car increases, the absolute value of the radial velocity increases, the variation gradient of velocity increases, the positive radial velocity area increases, and the boundary of the positive and negative radial velocity area distribution gradually becomes fuzzy. The circumferential flow velocity of the front section is distributed between −0.70 m/s and 0.62 m/s. When the load of the piped car increases, the absolute value of the circumferential velocity increases, the variation gradient of velocity increases, the distribution of the positive and negative circumferential velocity is regionally obvious, and the negative circumferential velocity area increases. The increase in load has a greater effect on axial velocity, radial velocity, and circumferential velocity when the piped car starts.
2. Characteristics of flow velocity in the ring gap section: When the piped car models are the same, axial velocity, radial velocity, and circumferential velocity have a 120° rotational symmetric distribution around the center of the cross section. The axial flow velocities of the annulus sections are all distributed in the range of −0.20 m/s to 2.37 m/s. When the load increases, the axial velocity increases, the variation gradient of velocity increases, and the contour spacing becomes smaller and more densely distributed. The radial flow velocity of the annular section is distributed between −0.55 m/s and 0.19 m/s. When the load of the piped car increases, the positive radial velocity increases, the negative radial velocity decreases, and the variation gradient of velocity increases. The circumferential flow velocity in the annular region of the annular section is distributed between −0.30 m/s and 0.34 m/s. When the load of the piped car increases, the absolute value of circumferential velocity increases, the variation gradient of velocity increases, and the flow velocity contour becomes densely distributed. The increase in load has a greater effect on axial velocity, radial velocity, and circumferential velocity when the piped car starts.
3. Characteristics of flow velocity in the rear of the car: The axial velocity of the rear section is distributed between −0.60 m/s and 2.20 m/s. When the piped car load increases, the axial velocity presents a symmetric distribution of a 120° rotation around the center of the cross section, and the regional demarcation of the velocity is more obvious. Furthermore, the average value of the axial velocity in the high-flow-velocity area behind the car increases, and the variation gradient of velocity increases. The radial flow velocity of the rear section is distributed between −0.45 m/s and 0.50 m/s. When the load of the piped car increases, the absolute value of the radial velocity increases, and the positive and negative flow velocity distributions are obvious in this region. The circumferential flow velocity of the rear section is distributed between −0.60 m/s and 1.29 m/s. When the load of the piped car increases, the absolute value of the circumferential velocity increases, the variation gradient of velocity increases, and the positive circumferential velocity area increases. The regional distribution of flow velocity is more obvious. The increase in load has a greater effect on axial velocity, radial velocity, and circumferential velocity when the piped car starts.

Author Contributions: Conceptualization, Y.L. (Yifan Lu) and X.S.; validation, Y.L. (Yifan Lu), X.S. and C.W.; formal analysis, Y.L. (Yongye Li); investigation, Y.L. (Yongye Li) and X.S.; data curation, Y.L. (Yifan Lu) and C.W.; writing—original draft preparation, Y.L. (Yifan Lu); writing—review and editing, Y.L. (Yifan Lu) and S.T.; funding acquisition, Y.L. (Yifan Lu) and Y.L. (Yifan Lu). All authors have read and agreed to the published version of the manuscript.

Funding: This research was funded by the National Natural Science Foundation of China (51179116, 51109155, 50579044) and the Natural Science Foundation of Shanxi Province (2015011067, 201701D221137).

Data Availability Statement: The data used to support the findings of this study are available from the corresponding authors upon request.

Acknowledgments: This research was supported by the Collaborative Innovation Center of New Technology of Water-Saving and Secure and Efficient Operation of Long-Distance Water Transfer Project at the Taiyuan University of Technology.

Conflicts of Interest: The authors declare no conflicts of interest.

References

1. Zhang, W.; Wu, S.; Ji, H.; Kolbe, H. Estimation of Agricultural Non-Point Source Pollution in China and the Alleviating StrategiesI. Estimation of Agricultural Non-Point Source Pollution in China in Early 21 Century. *Sci. Agric. Sin.* **2004**, *7*, 1008–1017.
2. Wang, Y.; Sheng, L.; Li, K.; Sun, H. Analysis of present situation of water resources and countermeasures for sustainble development in China. *J. Water Resour. Water Eng.* **2008**, *3*, 10–14.
3. Han, Y. Weak Magnetic Technology and Application on Pipeline Ontology Defect Testing. *Pipeline Tech. Equip.* **2019**, *3*, 27–30.
4. Li, Y.; Pang, Y.; Song, X.; Jia, X.; Lu, Y.; Sun, X.; Zhang, X. Influence of setting angle for guide bar on velocity characteristics of spiral flow in cross-sections between piped carriages. *Trans. Chin. Soc. Agric. Eng.* **2021**, *37*, 87–94.
5. Sun, X.; Li, Y.; Yan, Q. Experimental study on the starting conditions of hydraulic conveying piped car for cylinder loading pipelines. *National Symposium Hydrodynamics* **2006**, *8*, 417–423.
6. Ellis, H. The pipeline flow of capsules: Part 3-An experimental investigation of the transport by water of single cylindrical and spherical capsules with density equal to that of the water. *Can. J. Chem. Eng.* **1964**, *42*, 1–8. [CrossRef]
7. Kroonenberg, H. A mathematical model for concentric horizontal capsule transport. *Can. J. Chem. Eng.* **1978**, *56*, 538–543. [CrossRef]
8. Ma, H.; Kuo, C. Control of boundary layer flow and lock-on of wake behind a circular cylinder with a normal slit. *Eur. J. Mech. B-Fluids* **2016**, *59*, 99–114. [CrossRef]
9. Ihab, G.; Sadek, Z.; Mohamed, F.; Mohamed, A. Turbulent flow around single concentric long capsule in a pipe. *Appl. Math. Model.* **2010**, *34*, 2000–2017.
10. Ivanov, V.; Sokolov, S.; Ogudova, E. Methods of increasing efficiency and maintainability of pipeline systems. *IOP Conf. Ser. Mater. Sci. Eng.* **2018**, *357*, 012016. [CrossRef]
11. Sultan, A.; Rahman, A.; Rushd, S. Validation of CFD model of multiphase flow through pipeline and annular geometries. *Part. Sci. Technol.* **2019**, *37*, 681–693. [CrossRef]
12. Peng, W.; Xu, K.; Miao, Y. Experimental and CFD investigation of flow behavior and sand erosion pattern in a horizontal pipe bend under annular flow. *Particuology* **2023**, *75*, 11–25. [CrossRef]
13. Cheng, Z.; Li, J.; Chen, Z.; Chen, J.; Fan, R.; Liu, H. Study on numerical simulation of fluid flow in a sudden shrinking circular tube. *Chem. Eng. Equip.* **2021**, *11*, 3–6.
14. Jiang, F.; Huang, H.; Chen, M.; Huang, H. Study on Interfacial Fluctuation of Oil-water Annular Flow in Sudden Contraction Pipe. *J. Ningxia Univ. (Nat. Sci. Ed.)* **2023**, *44*, 226–233.
15. Paul, A.; Bhattacharyya, S. Analysis and Design for Hydraulic Pipeline Carrying Capsule Train. *J. Pipeline Syst. Eng. Pract.* **2021**, *12*, 04021003. [CrossRef]
16. Asim, T.; Mishra, R. Computational fluid dynamics based optimal design of hydraulic capsule pipelines transporting cylindrical capsules. *Powder Technol.* **2016**, *295*, 180–201. [CrossRef]
17. Asim, T.; Mishra, R.; Abushaala, S.; Jain, A. Development of a design methodology for hydraulic pipelines carrying rectangular capsules. *Int. J. Press. Vessel. Pip.* **2016**, *146*, 111–128. [CrossRef]
18. Lenau, C.; El-Bayya, M. Unsteady flow in hydraulic capsule pipeline. *J. Eng. Mech.* **1996**, *122*, 1168–1173. [CrossRef]
19. Zhang, C.; Sun, X.; Li, Y.; Zhang, X. Numerical simulation of hydraulic characteristics of cyclical slit flow with moving boundary of tube-contained raw materials pipelines hydraulic transportation. *Trans. Chin. Soc. Agric. Eng.* **2017**, *30*, 76–85.
20. Zhao, Y.; Li, Y.; Sun, X. Transient Model for the Hydrodynamic Force in a Hydraulic Capsule Pipeline Transport System. *Sustainability* **2023**, *15*, 15575. [CrossRef]
21. Zhao, Y.; Li, Y.; Sun, X. Modal Analysis of the Hydrodynamic Force of a Capsule in a Hydraulic Capsule Pipeline. *J. Mar. Sci. Eng.* **2023**, *11*, 1738. [CrossRef]
22. Turkowski, M.; Szudarek, M. Pipeline system for transporting consumer goods, parcels and mail in capsules. *Tunn. Undergr. Space Technol. Inc. Trenchless Technol. Res.* **2019**, *93*, 103057. [CrossRef]

23. Asim, T.; Algadi, A.; Mishra, R. Effect of capsule shape on hydrodynamic characteristics and optimal design of hydraulic capsule pipelines. *J. Pet. Sci. Eng.* **2018**, *161*, 390–408. [CrossRef]
24. Yang, X.; Ma, J. The Wall Stress of the Capsule Surface in the Straight Pipe. *Water* **2020**, *12*, 242. [CrossRef]
25. Taimoor, A.; Rakesh, M.; Kuldip, U. Optimal Design of Capsule Transporting Pipeline carrying Spherical Capsules. *J. Phys.* **2012**, *364*, 012070.
26. Ulusarslan, D.; Teke, I. Comparison of Pressure Gradient Correlations for the Spherical Capsule Train Flow. *Part. Sci. Technol.* **2008**, *26*, 285–295. [CrossRef]
27. Ulusarslan, D. Analysis of the Pressure Gradients According to Capsule Flow Mechanism. *Part. Part. Syst. Charact.* **2012**, *29*, 167–177. [CrossRef]
28. Deniz, U. Effect of Capsule Density and Concentration on Pressure Drops of Spherical Capsule Train Conveyed by Water. *J. Fluids Eng.* **2010**, *132*, 011304.

Disclaimer/Publisher's Note: The statements, opinions and data contained in all publications are solely those of the individual author(s) and contributor(s) and not of MDPI and/or the editor(s). MDPI and/or the editor(s) disclaim responsibility for any injury to people or property resulting from any ideas, methods, instructions or products referred to in the content.